Allosteric nanobodies uncovered a role of hippocampal mGlu2 receptor homodimers in contextual fear consolidation.

Pauline Scholler, Damien Nevoltris, Dimitri de Bundel, Simon Bossi, David Moreno-Delgado, Xavier Rovira, Driss El Moustaine, Michaël Mathieu, Emilie Blanc, Heather Mclean, et al.

Allosteric nanobodies uncovered a role of hippocampal mGlu2 receptors in context fear consolidation

Pauline Scholler*[,1,2], Damien Nevoltris*[,2,3], Dimitri de Bundel[1], Simon Bossi[4], David Moreno-Delgado[1], Xavier Rovira[1], Driss El Moustaine[1], Michaël Mathieu[1], Emilie Blanc[1], Heather McLean[4], Elodie Dupuis[2], Gérard Mathis[2], Eric Trinquet[2], Hervé Daniel[4], Emmanuel Valjent[1], Daniel Baty[3], Patrick Chames[3,#], Philippe Rondard[1#], Jean-Philippe Pin[1#]

[1] Institut de Génomique Fonctionnelle, CNRS UMR5203, INSERM U1191, Univ. Montpellier, Montpellier, France
[2] Cisbio Bioassays, Codolet, France
[3] Aix Marseille Univ, CNRS, INSERM, Institut Paoli-Calmettes, CRCM, Marseille, F-13009, France
[4] CNRS UMR9197, Université Paris-Sud, Institut des Neurosciences Paris-Saclay, France.

* Equal contribution
[#] To whom correspondence should be addressed.

Abstract

Antibodies have enormous therapeutic and biotechnology potential. G protein-coupled receptors (GPCRs), one of the main targets in drug development, are of major interest in antibody development programs. Metabotropic glutamate receptors are dimeric GPCRs that can control synaptic activity in a multitude of ways. Here we identify llama nanobodies that specifically recognize mGlu2 receptors, among the eight subtypes of mGluR subunits. Two of these nanobodies act as positive allosteric modulators (PAMs) on homodimeric mGlu2. One of them potentiates agonist actions on activated mGlu2, but has no effect on mGlu2-4 heterodimers. This PAM enhances the inhibitory action of the orthosteric mGlu2/mGlu3 agonist, DCG-IV, at mossy fiber terminals in the CA3 region of hippocampal slices. It also impairs contextual fear memory demonstrating for the first time the functional role of mGlu2 homodimers in living animals. These data also highlight the potential of developing antibodies with allosteric actions on GPCRs to better define their roles *in vivo*.

There is growing interest in developing either activating or inactivating antibodies with therapeutic potential[1,2], but also as innovative tools to decipher the functional roles of cell surface proteins[3]. G protein-coupled receptors (GPCRs), that are the main targets for small therapeutic molecules, are now considered as promising targets for therapeutic antibodies[4-7]. Single chain antibodies from camelids, such as llamas, are particularly well suited for such purposes, being more prone to target specific conformations of their targets[6,8,9]. Such tools have already proven their potential for pharmacological actions[6,10], structural studies[8,11], and use as biosensors[3].

In the central nervous system, glutamate, the main excitatory neurotransmitter, exerts its fast actions via ionotropic receptors, but also modulates synaptic activity via GPCRs, so called metabotropic glutamate receptors (mGluRs)[12-14]. Eight genes encoding mGluRs are found in mammalian genomes, and are classified into three groups. While group-I receptors (mGlu1 and mGlu5) are mainly post-synaptic receptors that contribute to glutamatergic synaptic responses, group-II (mGlu2 and 3) and -III (mGlu4, 6, 7 and 8) are mainly pre-synaptically located, and inhibit transmitter release at various types of synapses[12]. As such, mGluRs are considered to be interesting targets for the treatment of various brain diseases including psychiatric or neurodegenerative diseases[12,13].

Among the various mGluR subtypes, mGlu2, but also mGlu3 and 5, open new possibilities for novel antipsychotic drugs[13,15]. However studies on the roles of mGlu2 are made difficult by the limited number of specific tools. Indeed, there are no specific mGlu2 antibodies to determine their precise localization in the brain[16]. Moreover, because of the high conservation of the orthosteric glutamate binding site located in the Venus flytrap extracellular domain (VFT) of these receptors[17], only very few selective agonists have been reported[18,19]. Efforts were concentrated on the development of positive allosteric modulators (PAMs) interacting with the less conserved 7 transmembrane domains (7TM)[17]. Although subtype selective PAMs have been identified, a number of limitations for their development have been observed[20,21]. Although knock out lines are available[12,13], one cannot exclude compensation during development. Eventually, mGluRs, and especially mGlu2 have been reported to associate with other mGlu subunits to form heterodimers[22-24], and evidence for mGlu2-4 heterodimers in cortico-striatal terminals have recently been provided[23]. These observations strengthen the need for more specific tools to better characterize the functional roles of homo or heterodimeric mGluRs containing the mGlu2 subunit.

In the present study, we aimed at identifying nanobodies[25,26] that recognize specific conformations of the mGlu2 receptor. This led us to identify two nanobodies that specifically bind to the active form of the mGlu2. Accordingly, these nanobodies act as PAMs, enhancing the agonist action at mGlu2 receptors in transfected cells and in brain slices. When injected in the hippocampus, these nanobodies also enhance the effect of a group-II mGluR agonist in the fear-conditioning test, demonstrating their possible use to decipher the physiological role of mGlu2 receptors in the brain. These data nicely illustrate novel possibilities to develop mGlu allosteric modulators for numerous therapeutic actions, and exemplify the use of nanobodies to allosterically modulate GPCRs.

Results:

Identification of mGlu2 selective nanobodies

To identify nanobodies recognizing mGlu2 receptors, HEK-293 cells transiently expressing both rat and human mGlu2 were injected in llamas, and VHH encoding sequences were amplified to generate a phage display library[27]. By screening the later using a purified mGlu2 receptor reconstituted into nanodiscs, several positive clones were isolated and three of them, DN1, DN10 and DN13 were retained for analysis. FRET based binding data (Fig. 1a) revealed that all three nanobodies bind to mGlu2 in the presence of ambient glutamate produced by the cells, and not to any other mGluR (Fig. 1b).

Because glutamate concentration in the blood is sufficient to fully activate mGlu2 receptors, we expected that some of our identified nanobodies could preferentially bind to the active form of the receptor (Fig 1c). Indeed, whereas DN1 displays the same affinity for the active and inactive forms of mGlu2 (Fig. 1d and Supplementary Table 1), DN10 and DN13 specifically bind to the active form stabilized by the orthosteric agonist, LY379268 (Fig. 1e,f and Supplementary Table 1). No binding was detected on the inactive form of the receptor in the presence of the antagonist LY341495 (Fig. 1e,f). Note that in the absence of any added ligand, and under conditions leading to very low extracellular glutamate concentrations in the assay medium through the co-transfection of the receptor with the high affinity glutamate transporter EAAC1, no binding of DN10 and DN13 to mGlu2 could be detected (Supplementary Fig. 1a). This is in contrast to the conditions used for the screening and first characterization of the nanobodies where binding could be detected under basal condition, likely due to the presence of enough glutamate produced by the cells in the assay (Fig. 1b). According to these data, the specificity of both DN10 and DN13 was further examined on the eight mGlu subtypes in the presence of a saturating concentration of either agonists or antagonists (Supplementary Fig. 1b and 1c, respectively). It demonstrated that these two nanobodies only bind on the active form of mGlu2 receptor.

DN10 and DN13 are positive allosteric modulators of mGlu2

A possible effect of both DN10 and DN13 was first examined using a mGlu2 biosensor[28]. This sensor makes use of the large movement between the VFTs that occurs upon receptor activation, leading to an increase in distance between the N-terminal SNAP tags carried by each subunit[28]. Such movement lead to a large decrease in lanthanide-based resonance energy transfer (LRET) measured in a time resolved manner (TR-FRET) (Fig. 2a). In the presence of an EC_{20} concentration of LY379268, both DN10 and DN13 were found to activate the biosensor in the high nanomolar range (Fig. 2b). A similar agonist effect of both DN10 and DN13 was observed using a functional assay based on the activation of phospholipase C by this Gi/o-coupled receptor using a chimeric Gqi protein (Supplementary Fig. 2). When the extracellular glutamate concentration was maintained as low as possible using EAAC1, both DN10 and DN13 clearly increased mGlu2 agonist LY379268 potency (Fig. 2c,d), revealing their positive allosteric effect. However, whereas DN13 retains minimal agonist activity under such conditions (Fig. 2d), DN10 was still able to activate mGlu2 (Fig. 2c). Such observations were confirmed using the inositol-phosphate accumulation assay (Fig. 2e,f). These data demonstrate that both DN10 and DN13 act as PAMs on mGlu2, but that DN10 has, in addition, an intrinsic agonist activity (known as ago-PAM[29]).

DN13 binds at an epitope specific of the active conformation

The binding ability of the nanobodies on various mGlu2 constructs lacking the 7TM domains, the cysteine-rich domain, or the entire extracellular domain, revealed that all three nanobodies bind to the VFT (Supplementary Fig. 3). Moreover, competition studies revealed that DN10 and DN13 share part of their binding epitope, while DN1 binds at a different site (Supplementary Fig. 4). To identify the epitope recognized by DN13, we made use of the inability of these nanobodies to bind to the homologous mGlu3 receptor, and their lack of affinity for the inactive form of the receptor. The major conformational change in the VFT dimer occurring upon receptor activation is the relative reorientation of the VFTs leading to a close apposition of the second lobes, which are distant in the inactive form (Fig. 1c)[28]. Accordingly, a specific crevice at the interface of the second lobes is formed in the active form of the dimer only, and a few residues in that area were found to be different between mGlu2 and mGlu3 receptors (Fig. 3a-c and Supplementary Table 2). These include Leu226, Arg445 and Ile450 in protomer A (Fig. 3c) (Gln, Thr and Met in mGlu3, respectively), and Ser246, Ala248, Ala249, Glu251 and Gly252 in protomer B (Ile, Lys, Ser, Asp and Ser in mGlu3, respectively). Docking experiments conducted with a 3D model of DN13 and a mGlu2 VFT dimer model suggest that DN13 interacts at that site (Fig. 3a-c). This is further demonstrated by our observation that DN13 does not interact with a mGlu2 mutant in which these residues were replaced by their mGlu3 equivalent (Fig. 3d and Supplementary Table 3) despite their normal expression and coupling properties (Supplementary Fig 5). In contrast, DN13 binds with a nanomolar affinity on the mGlu3 mutant bearing these residues from mGlu2 (Fig. 3e and Supplementary Table 3).

There is increasing evidence suggesting that mGlu2 receptors can exist not only as homodimers, but also as heterodimers, associated with any group-III mGluRs[22,23]. Because the epitope recognized by DN13 involves both subunits in the mGlu dimer, we predicted that it would be specific for the mGlu2 homodimer relative to the heterodimers made of mGlu2 and a group-III mGlu subunits. Indeed, DN13 did not bind to the mGlu2-4 heterodimer (Supplementary Fig. 6a), nor did it potentiate agonist action on this heterodimer as revealed using either a mGlu2-4 specific biosensor, and a functional assay using subunit combination that ensure targeting to the cell surface of the heterodimer only[30] (Supplementary Fig. 6b,c).

DN13 potentiates the pre-synaptic effect of mGlu2

The mGlu2 gene is well expressed in hippocampal dentate gyrus granule neurons, where the receptors are targeted to mossy fiber terminals that contact pyramidal neurons in the CA3 area (Fig. 4a). These terminals may also contain mGlu3, mGlu4 and mGlu7 that are also expressed by granule neurons[31,32]. In acute hippocampal slices, we examined the effect of nanobodies on mossy fiber terminal mGlu2 activation by quantifying presynaptic calcium transients evoked by electrical stimulation of mossy fibers, using photometric measurements of the fluorescent Ca^{2+} sensitive dye, magnesium green-AM[33]. We found that saturating concentrations of DN13 (2.5 µM), did not affect the amplitude of Ca^{2+} transients in mossy fiber terminals when applied alone but clearly enhanced the inhibitory effect of low concentrations (100 nM) of the group-II mGluR agonist DCG-IV (24 ± 1.4 % and 8.3 ± 0.9 % inhibition with and without DN13, respectively, $p < 0.001$, $n = 9$) (Fig. 4b). In the presence of DN13, the effect of a low concentration of DCG-IV nearly reached the maximal effect observed with saturating concentrations of the drug (30.5 ± 1.9 %, $n = 6$). In addition, and as

175 expected for a PAM effect, the off rate of the inhibitory action of a saturating concentration of
176 DCG-IV (5 μM) is prolonged in the presence of DN13 (Supplementary Fig. 7).

177 The hippocampal mossy fiber pathway projecting from the dentate gyrus to the CA3 is
178 critically involved in memory processing. Infusion of the group-II mGluR agonist DCG-IV into
179 the CA3 area was previously shown to block contextual fear memory consolidation in mice[34].
180 Consistent with this observation we found that DCG-IV infused into the CA3 area (Fig. 4d
181 and supplementary Fig. 8) specifically disrupted contextual fear memory consolidation (Fig.
182 4e) without affecting cued fear memory consolidation (Fig. 4f) when immediately following
183 conditioning (Fig. 4c). DN13 did not affect fear memory consolidation when applied alone,
184 but potentiated the effect of low concentrations of DCG-IV, demonstrating the involvement of
185 mGlu2 (Fig. 4e).

186

Discussion

In the present study, we describe three nanobodies that specifically recognize mGlu2 in the nanomolar range, being then the first mGlu2 selective antibodies. Most interestingly, while one of these does not discriminate between the different conformations of the receptor, the two others, DN10 and DN13 exclusively bind to the active form, interacting at a site exclusively found in the active form of the dimer. In the study we have further characterized the DN13 nanobody that behaves as a PAM with no intrinsic agonist activity. Indeed, DN13 potentiated the action of mGlu2 agonists not only in heterologous expression systems, but also in brain slices and *in vivo.* Because the binding epitope of DN13 involves residues from both subunits, it is indeed inactive on mGlu2-4 heterodimers, indicating that the effects observed both in brain slices and *in vivo* at the level of the hippocampal CA3 area likely involves mGlu2 homodimers.

Despite the identification of both mGlu2 and mGlu3 in the early 90's, and the interest they have generated for the development of anxiolytic and antipsychotic drugs, studies of these two receptors have been hampered by the lack of specific pharmacological tools. Until now, available antibodies have not been able to discriminate between mGlu2 and mGlu3[16], and only few selective ligands have been developed[18,19]. However, the availability of mGlu2 and mGlu3 knockout mice (or mouse lines) coupled with more sophisticated pharmacology has strengthened the interest in targeting mGlu2 specifically for antipsychotic effects[35]. Today, the most selective and promising ligands are mGlu2 PAMs that bind to a hydrophobic cavity in the 7TM[36]. Accordingly, such molecules show high hydrophobicity enabling them to pass through the blood brain barrier. However, this also limits their effective concentration in the cerebrospinal fluid, and increases the chance for off target activity[20]. Despite the therapeutic potential of PAMs, so far only orthosteric mGlu2-3 agonists have reached phase 3 clinical trails for anxiety and schizophrenia[35] but have had very limited success. Our nanobodies are the first mGlu2 selective PAMs that do not target the 7TM domain, but rather the VFT domain. These molecules reveal new possibilities to develop selective mGlu2 PAMs that are designed to target this new site, without the limiting hydrophobic properties.

Although mGluRs were thought to exist exclusively as homodimers, recent data has revealed that both group-I, and group-II/III mGluRs can associate to form multiple types of heterodimers[22]. Among these, the heterodimeric mGlu2-4 receptor is likely present in striato-cortical terminals, as illustrated by co-immunoprecipitation experiments, and the selective action of one mGlu4 PAM[23]. This is in agreement with our observation that DN13 interacts with both subunits in the mGlu2 VFT dimer and was found to be inactive on the mGlu2-4 heterodimer. This finding will lead to multiple possibilities to develop selective nanobodies for mGlu homo and heterodimers comprised of specific mGlu subunits.

Although group-II mGluR agonists are well known for their anxiolytic and antipsychotic properties, recent data also suggest that they act to consolidate context fear memory[34]. This may result from a reduction in pre-synaptic glutamate release following activation of group-II mGluRs located at the mossy fiber terminals in the CA3 area of the hippocampus. These terminals originate from the granule neurons of the dentate gyrus that also express mGlu3[16] and as such, that the inhibitory action of the group-II agonist DCG-IV reported at these synapses may involve either mGlu2 or mGlu3. Our data using DN13, an mGlu2 selective PAM, suggest that only mGlu2 receptors are involved in the DCG-IV effect. Eventually, the DN13-mediated potentiation of the DCG-IV effect confirmed that a selective

activation of mGlu2 can prevent the consolidation of context fear memory. These data also argue against the involvement of an mGlu2 receptor heterodimer containing mGlu4, and likely the other group-III mGlu7 subunit both expressed in hippocampal granule neurons[16,31,32].

Taken together, our data are the first to report the development of PAM nanobodies acting at a GPCR. Antibodies show increasing potential in therapeutics, although mainly by targeting proteins other than GPCRs[1]. Since GPCRs still represent important targets for therapeutic interventions, these membrane receptors have only recently been highlighted as possible targets for antibody-based biologics[4,5]. So far, such possibilities have been validated through the identification of antibodies inhibiting chemokine receptors[4,6]. Here we extend the use of this approach revealing the feasibility to develop nanobodies with very selective PAM activity at mGlu2 GPCRs, thus offering a way to better identify their actions *in vivo*, as well as localizing activated receptors within the brain. Although an access to the brain would be needed for targeting these central receptors for therapeutic intervention, conditions have been reported to facilitate brain penetration of nanobodies[37]. Moreover, mGlu receptors are not only expressed in the CNS, but also at the periphery where they have a role in the regulation of cardiovascular[38] and immune systems[39], as well as in cancer[40]. Taken together, mGluR targeting nanobodies offer interesting possibilities for therapeutic intervention.

Acknowledgements

We thank L Prézeau, D Maurel and C Vol from ARPEGE (Pharmacology Screening-Interactome) facility at the Institut de Génomique Fonctionnelle (Montpellier, France) for their help in various microplate assays. Funding was provided by the Centre National de la Recherche Scientifique (CNRS), the Institut National de la Santé et de la Recherche Médicale (INSERM), the University of Montpellier, Cisbio Bioassays, the Fondation Recherche Médicale (FRM DEQ20130326522) and the Fondation Bettencourt Schueller to JPP; the Fond Unique Interministériel of the french government (FUI, Cell2Lead project) to GM, JPP and DB; the Agence Nationale de la Recherche (ANR-15-CE18-0020-01) to PR.

Author Contributions:

JPP, PR, PC, DB, EV, HD, HML, ET, GM, ED designed the research.

DN generated the nanobody phage display library and performed the screening and primary characterization of the nanobodies, DEM set up the conditions and prepared the purified mGlu2 receptor in nanodiscs, PS, DMD, MM, EB performed the *in vitro* characterization of the nanobodies, XR performed the *in silico* studies, SB performed the experiments on hippocampal slices, DDB performed the *in vivo* experiments.

JPP, PR and PS wrote the paper, with inputs from HML, PC and EV.

Author Information

The authors declare competing financial interests. Correspondence and requests for materials should be addressed to JPP (jean-philippe.pin@igf.cnrs.fr), PR (philippe.rondard@igf.cnrs.fr) or PC (patrick.chames@inserm.fr)

Figure legends:

Figure 1: Nanobodies DN1, DN10 and DN13 specifically interact with mGlu2 receptors. **a)** Cartoon illustrating the principle of the TR-FRET binding assay. The receptor fused to a SNAP-tag (black circled labeled "S") is labeled with Lumi4-Tb (light blue ball) while the nanobody (purple) bearing a c-Myc epitope at its C-terminus is labeled with 200 nM of anti-c-Myc antibody (green) coupled to d2 fluorophores (orange). Binding of the nanobody to the receptor is then measured by a TR-FRET signal. **b)** Specific TR-FRET binding data obtained with the indicated mGlu receptor and either DN1, DN10, DN13 or a control irrelevant nanobody in cells under basal condition with ambient glutamate. Data are mean ± SD of triplicates from a typical experiment representative of three experiments. **c)** Cartoon illustrating the main active (left), and inactive (right) conformation of an mGlu2 dimer, stabilized by an agonist (glutamate or LY379268) or the antagonist LY341495, respectively. **d,e,f)** Saturation binding curves obtained with DN1 (**d**), DN10 (**e**) and DN13 (**f**) on mGlu2 receptors under control conditions with low extracellular glutamate thanks to the co-expression of the high affinity glutamate transporter EAAC1 (buffer), in the presence of the agonist LY379268 (1 µM), or the antagonist LY341495 (10 µM). Data are mean ± sem of three individual experiments each performed in triplicates.

Figure 2: DN10 and DN13 are positive allosteric modulators of mGlu2. **a)** Cartoon illustrating the principle of the mGlu2 sensor assay, where the VFT movement associated with receptor activation results in a decrease in TR-FRET signal measured between Lumi4-Tb and SNAP-Green labeled SNAP tags. **b)** DN10 and DN13 concentration dependent decrease the sensor signal in the presence of EC_{20} concentration of agonist LY379268 (0.1 nM), indicative of receptor activation. DN10 **(c)** and DN13 **(d)** dose-dependently potentiate the effect of LY379268 on the mGlu2 sensor. DN10 **(e)** and DN13 **(f)** dose-dependently potentiate the effect of LY379268 on the production of inositol phosphate in mGlu2-transfected cells. Note that the lower the IP-One Gq HTRF® ratio, the higher the amount of inositol monophosphate produced (IP1). Data are means ± sem of three individual experiments each performed in triplicates.

Figure 3: DN13 interacts at the lobe 2 crevice on the activated mGlu2 VFT dimer. **a-b)** View of the proposed docking of DN13 (orange) on the mGlu2 extracellular domain dimer (*a*, lateral view, *b*, top view). **c)** Detailed view of the proposed docking of DN13 illustrating proposed residues involved in selectivity, shown are Leu226 and Arg445 in protomer A, and Ser246, Ala248 (yellow), Ala249, and Glu251 from protomer B. **d)** Saturation binding curves of DN13 on mGlu2 WT, mGlu2 bearing mGlu3 specific residues from protomer A (mut A), mGlu2 bearing mGlu3 residues from protomer B (mut B), mGlu2 A248K mutant. **e)** Saturation binding curves of DN13 on mGlu3 WT, mGlu3 bearing the mGlu2 residues on protomer A (mut A), and mGlu3 bearing all identified residues of mGlu2 (mut AB). Data are mean ± SD of triplicates from a typical experiment representative of three experiments.

Figure 4: mGlu2 receptors in the CA3 area of the hippocampus control contextual fear consolidation. **a)** A schematic view of the hippocampus illustrating the granule neurons of the dentate gyrus (DG) projecting to the pyramidal neurons in the CA3 area via the mossy fibers. **b)** DN13 potentiates the inhibitory effect of a mGlu2-mGlu3 agonist (DCG-IV, 100 nM) on presynaptic evoked calcium transients in the CA3 area (red box in panel *a*) in response to

electrical stimulation of the mossy fibers (blue arrow head in panel *a*). Data are normalized amplitudes of peak fluorescence transients (ΔF/F) evoked by five stimulations of mossy fibers (delivered at 100 Hz). Insert on the right shows the average normalized area corresponding to the depressant effect of DCG-IV alone (black bar, 100 ± 5.4%, n=10) and in the presence of DN13 (white bar, 578.5 ± 69%, n=9), $p<0.001$. Insert on the left displays superimposed fluorescence changes in one of these experiments recorded at the indicated times. Each trace is an average of 10 consecutive trials. Since the variance was different between DCG-IV and DCG-IV + DN13 groups, the Welch test was applied for statistical analysis. **c)** Schematic of the experimental protocol used for the contextual fear consolidation examination in mice, and drug infusion site **(d)**. **(e)** Contextual fear memory expression ANOVA: $F_{5,35} = 6.025$, $P = 0.0004$. **(f)** Cued fear memory. ANOVA: $F_{5,35} = 0.3053$, $P = 0.9066$. * $P < 0.05$ vs PBS and ** $P < 0.01$ vs PBS.

Methods

Reagents, cell lines, antibodies and plasmids

HEK293 cells were cultivated in DMEM (Thermo Fischer Scientific, Courtaboeuf, France) complemented with 10% (v/v) fetal bovine serum. All drugs (DCG-IV, LY341495, LY379268, LY487379) were from Tocris Bioscience (Bristol, UK). All HTRF® reagents, labeled monoclonal antibodies Anti-c-myc-d2 and Anti-6His-d2, labeled ligands (SNAP-Lumi4-Tb, SNAP-Red and CLIP-Red) and SNAP-tag mGluR plasmids, were a kind gift from Cisbio Bioassays (Codolet, France). The pRK5 plasmids encoding wild-type rat mGluR subunits, with a HA-tag and with SNAP or CLIP inserted just after the signal peptide, were previously described (Scholler et al Nat Chem Biol 2017). Point mutations were introduced in the SNAP-tag mGlu2 or mGlu3 plasmids according to the QuikChange mutagenesis protocol (Agilent Technologies, Santa Clara, CA, USA).

Llama immunization and library construction

Two llamas (Lama glama) were immunized subcutaneously 4 times with $5x10^7$ HEK293T cells transfected with rat mGluR2 and human mGluR2. VHH library constructions were performed in E. coli TG1 strain as previously described[27,41]. Library diversities were above 10^9 transformants.

Selection of nanobodies by phage display

20 µL of the bacteria library was grown in 50 mL of 2YTAG (2YT／ampicillin 100 µg/mL／2% glucose) at 37°C with shaking (250 rpm) to an OD_{600} between 0.5 and 0.7. Bacteria were infected by KM13 helper phage using a multiplicity of infection of 20 during 30 min at 37°C without shaking. The culture was centrifuged for 15 min at 3000 g, and bacterial pellet was re-suspended in 250 mL of 2YTA / kanamycine (50 µg/mL) for an overnight phage-nanobodies production at 30°C with shaking. The overnight culture was split in 10 vials and centrifuged for 20 min at 3000 g. Five mL of 80% PEG8000, 2.5 mM NaCl were added to the supernatant in a new clean vial and incubated for 1 h on ice to induce phage particle precipitation. The solution was centrifuged for 20 min at 3000 g at 4°C and the phage-containing pellet was re-suspended in 1 mL PBS. Another centrifugation step (2 min, 14000 g) was performed to eliminate bacterial contaminant, and 200 µL of PEG8000 NaCl was added to supernatants in a new vial. After 30 min on ice and a last centrifugation (5 min, 14000 g), phage-containing pellets were re-suspended in 1 mL PBS to obtain ready to used phage-nanobodies for selections.

To obtain mGluR2 specific clones, a first round of selection (S1) was performed on Maxisorp plates (Nunc, Maxisorp®) coated 24 h at 4°C with purified human mGlu2 receptor reconstituted in nanodiscs[42]. Before selection on purified mGluR2, phage-nanobodies library was depleted by incubation with empty nanodiscs (without receptor) to eliminate anti-nanodisc antibodies and to reduce non-specific binding. Remaining phages and purified mGluR2 coated wells were saturated with 2% milk/PBS during 1 h at 4°C, and then phages and antigen were incubated together during 2 h at 4°C for selection with shaking. Wells were then washed 10 times with PBS, and bound phages were finally eluted with 1 mg/ml trypsine solution (Sigma-Aldrich, Saint-Quentin Fallavier, France) during 30 min at room temperature with shaking. Phages were rescued and reamplified by infection of TG1 and phage production as above, yielding S1 polyclonal phage population.

To avoid non-specific selection against proteins that composed nanodics and to select antibodies against mGlu2 receptor in a cellular context, a second round of selection (S2) was

performed on HEK293T cells transfected with rat mGluR2 ($2x10^7$ cells). S1 polyclonal phage population and cells were saturated in 2% milk/PBS during 1 h at 4°C, and incubated together in the same conditions as described previously. After five PBS washes, bound phages were eluted using trypsin solution (1 mg/ml) during 30 min at room temperature. Phages were again rescued in TG1 and infected bacteria corresponding to S2 were plated. Individual TG1 colonies from S2 were picked and grown in two different 96-deep-well plates in 400 µL of 2YTAG. After overnight growth, half of the culture was frozen at -80°C in 20% glycerol for backup, and the rest of culture was used for soluble nanobodies production induced by isopropyl-β-26-D-thiogalactopyranoside (IPTG). Nanobody concentrations in supernatant were estimated at 100-500 nM using the DoubleTag check kit (Cisbio Bioassays) according to manufacturer's recommendations.

Production and purification of nanobodies

For large-scale nanobody production, positive phagemids from screening step were transformed in E. coli BL21DE3 strain. A single colony was grown into 10 ml of LB supplemented with 100 µg/mL ampicillin, 1% (wt/vol) glucose and 1 mM $MgCl_2$ overnight at 37°C with shaking. Then 1 L of LB supplemented with 100 µg/mL ampicillin, 0.1% (wt/vol) glucose and 1 mM $MgCl_2$ was inoculated with 10 ml of the preculture and incubated until an OD_{600} of 0.7. The nanobody expression was then induced with 1 mM IPTG (final concentration) and bacteria were grown overnight at 28°C with shaking. Bacteria were then collected by centrifugation for 10 min at 5,000 g, re-suspended in 15 mL of ice-cold TES buffer (0.2 M Tris, 0.5 mM EDTA, 0.5 M sucrose, pH 8), and incubated for at least 1 h at 4°C on a shaking platform. 30 mL of TES/4 buffer (TES buffer diluted 4 times in water) were then added to the solution and further incubated for at least 45 min at 4°C on a shaking platform. The periplasmic extract was recovered by collecting the supernatant after centrifugation of the suspension for 30 min at 10,000 g at 4°C. The His-tagged nanobodies were then purified from the periplasmic extract by using Ni-NTA purification (Qiagen, Hilden, Germany) according to the manufacturer's instructions.

Nanobody labeling

Nanobobies were dialysed overnight at 4°C and incubated (250 µg of nanobodies at 2 mg/ml) with the fluorophore-NHS (d2-NHS (Cisbio Bioassays, Codolet, France) into carbonate buffer pH 9, and Lumi4-Tb-NHS (Cisbio Bioassays, Codolet, France) in phosphate buffer 50 mM at pH 8, or acceptor and donor labeling, respectively) at a molar ratio of 6, for 45 min at room temperature. Nanobodies were then purified by gel filtration column (NAP-5) in phosphate buffer 100 mM pH 7. The final molar ratio (corresponding to the number of fluorophore per nanobodies) was calculated as the fluorophore concentration/conjugated nanobody concentration, and the conditions set up for a ratio between 2 and 3. The concentration of fluorophores in the labeled fraction was calculated as the OD/ε for each fluorophore (OD at 340 nm and ε=26,000 $M^{-1}.cm^{-1}$ for Lumi4-Tb, and OD at 650 nm and ε=225,000 $M^{-1}.cm^{-1}$ for d2), while that of nanobodies was determined by the OD_{280}. The conjugated concentration calculated as OD_{280}-($OD_{fluo}/R_z max$)/ε nanobody, with $R_z max=OD_{fluo}/OD_{280}$. Purified labeled fractions were supplemented with 0.1% BSA and kept at -20°C.

Time resolved fluorescence resonance energy transfer (TR-FRET) assay

Binding and competition experiments assays were performed using HEK-293 cells transfected with rat SNAP-tagged mGluR by electroporation as previously described[22]. 24 h

after transfection, cells were labeled with 300 nM SNAP-Lumi4-Tb in DMEM-GlutaMAX (Thermo Fischer Scientific) for 1 h at 37°C, and then washed three times with Krebs buffer. Depending on the experiments, either 100,000 cells per well were seeded in white 96-well plates (Greiner, Kremsmünster, Austria). For epitope mapping, cells were transfected with Lipofectamine 2000 (Thermo Fischer Scientific) according to the manufacturer's instructions. 20,000 cells/well were used for a white 384SV-well plates (Greiner). The His_6- and c-Myc-tagged nanobodies were incubated with the drugs and transfected cells and revealed by 200 nM of Anti-6His-d2 or Anti-c-myc-d2. When using d2 labeled nanobody, the anti-tag antibody was replaced by 5 µL of Krebs buffer. After 2h incubation at 4°C, d2 acceptor TR-FRET signal (665 nm) and Tb donor signal (620 nm) were measured using a 50 µs delay and a 450 µs integration upon excitation at 337 nm on a PHERAstar FS (BMG LabTech). TR-FRET ratio (665 nm / 620 nm x 10^4, Cisbio Bioassays patent US5,527,684) was calculated for preventing interference due to medium variability and chemical compound or to normalize experiments when using cells expressing different receptors levels.

For the mGlu2 TR-FRET biosensor, the SNAP-tagged mGlu2 homodimer was labeled with SNAP-Lumi4-Tb and SNAP-Red substrates as previously reported[28,30].

Measurement of inositol phosphate accumulation in HEK293 cells transiently expressing the mGlu receptors and a chimeric Gqi_9 protein (enabling the coupling of mGlu2 to the Gq pathway) after a 24 h transfection with Lipofectamine 2000 was determined using the IP-One Gq kit (Cisbio Bioassays) according to manufacturer's recommendations as previously described[43].

In silico analysis of DN13 binding site

The homology models of DN13 nanobody and the extracellular domain of $mGlu_2$ were generated with Modeller 9.12[44] based on the crystal structure of β_2-adrenoceptor bound nanobody (PDB 3P0G) and the $mGlu_3$ amino terminal domain as a template (PDB Code 2E4U) [45], respectively, using the loop optimization method. The sequences of template and modeled proteins were aligned with ClustalW2[46]. From 100 models generated, the top ten classified by DOPE score[47] were visually inspected and the best scored structure with suitable loops was chosen. The closed-closed $mGlu_2$ dimeric state was constructed by superimposition with the crystal structure of the active state of the extracellular domain of $mGlu_1$ (PDB code 1ISR)[48]. A comparison with the very recently published structure of $mGlu_2$ in active state (PDB code 4XAS)[49] demonstrates a close similarity with a Cα RMSD of 1.36 for the dimer and 0.86 for the monomer. The maximum structural divergence is found in the loops whereas the parts analyzed in the mutational study are very accurately located in the model.

A docking based approach was used to find the binding site of DN13 nanobody in mGlu2 according to a previously described methodology[50]. Briefly, ZDOCK 3.0 program [51] was used to perform an exhaustive rigid-body search in the six-dimensional rotational and translational space. The three rotational angles were sampled with 6° spacing, and the three translational degrees of freedom were sampled with a 1.2 Å spacing. For each set of rotational angles, only the best translationally sampled prediction was retained resulting in 54,000 predictions. The 2,000 first ranked predictions were clustered with MMTSB Tool Set[52] using K-means and a radius of 2.5 Å. The ten most populated clustered were visually inspected to avoid structural violations and symmetric results. Discovery Studio 4.0 (BIOVIA – A Dassault Systèmes brand – 5005 Wateridge Vista Drive, San Diego, CA 92121 USA) was used for protein structure visualization and PDB file editing purposes. Images were generated with

UCSF Chimera software[53]. The multiple sequence alignment visualization and analysis was performed with Jalview2 software[54].

Slice preparation and calcium transient recordings

Experiments were performed using hippocampal slices prepared from twenty six 21-25 day-old male Sprague-Dawley rats. No experiments were excluded from the analysis. In accordance with guidelines from the Centre National de la Recherche scientifique (CNRS, France), animals were killed by decapitation after anesthesia with 2-bromo-2-chloro-1, 1, 1-trifluoroethan, and the brain was removed rapidly and put in an ice-cold cutting solution (75 mM sucrose, 25 mM glucose, 25 mM $NaHCO_3$, 2.5 mM KCl, 87 mM NaCl, 1.25 mM KH_2PO_4, 7mM $MgCl_2$, 0.5 mM $CaCl_2$). Parasagittal hippocampal slices, 350 µm thick, were prepared using a Vibroslicer (Motorised Advance Vibroslice MA752, Campden Instruments) according to [55]. Slices were then placed in oxygenated (saturated with 95% O_2 and 5% CO_2) artificial CSF (138.6 mM NaCl, 3 mM KCl, 1.15 mM KH_2PO_4, 1.15 mM $MgSO_4$, 24 mM $NaHCO_3$, 2 mM $CaCl_2$, 10 mM glucose) and left to recover at room temperature for at least 1 h. Slices were then transferred to the recording chamber, where they were maintained at 29–30°C and perfused with oxygenated artificial CSF as above.

Presynaptic calcium transients were recorded by photometry according to Regehr and collaborators[33,56]. A solution of 100 µM of the membrane-permeant calcium dye Magnesium Green-AM was delivered during 40 min at the level of the stratum lucidum in CA3, where mossy fibers contact proximal dendrites from pyramidal cells. After loading of the mossy fiber, slices were left for at least 30 min to allow diffusion of the fluorochrome in the fibers. A stimulation electrode filled with artificial CSF was placed between the fluorochrome loading site and the measurement window. To measure the effect of mGlu2 ligands on evoked presynaptique calcium influx, a train of five 100 Hz stimulations is delivered every 30 s to the mossy fiber to induce presynaptic calcium transients, in the presence or absence of the indicated drugs or nanobodies. During acquisition, a $GABA_A$ receptor antagonist (bicuculline methiodide) was added to the artificial CSF to block any GABAergic component.

Measurements of intracellular calcium variations were performed on an epifluorescence microscope (Zeiss axioskop 2), with a mercury lamp (Mercury short Arc HBO, 103 W) for excitation (485 nm excitation filter), and a 530 nm emission filter. The measurement window was localized at some distance from the loading site, allowing the selective recording of loaded mossy fiber with a high signal to noise ratio. The basal fluorescence (F) and the amplitude of the fluorescence peak after mossy fiber stimulation (ΔF), and the $\Delta F/F$ ratio were measured in real time. Each recoding was then analyzed individually using Microsoft Excel before pooling them all together. Statistical significance was assessed by either an unpaired Student's t test or a Welch's t. The similarity of variance between each group of results was tested using Ficher's test with $\alpha = 0.02$. (n) indicates the number of cells included in the statistics.

Contextual fear memory

Cannula implantation. Mice were bilaterally implanted with an infusion cannulae (26 gauge, 2.5 mm, Plastics One, Roanoke, VA, USA) aimed at the dorsal hippocampal CA3 using flat skull coordinates: AP:-1.6 mm, ML ±2.5 mm, DV:-1.5 mm. The cannulae were fixed to the skull using anchor screws and acrylic dental cement (AgnTho's, Lidingö, Sweden). Following surgery, mice were placed on a heating mat and a dummy cannula was inserted into each guide cannula to seal off the opening. Mice were allowed to recover from surgery for a

minimum of one week during which time they were handled and habituated to the drug infusion procedure on a daily basis.

Fear conditioning. Pavlovian fear conditioning was performed in a conditioning box (20 cm width × 20 cm length × 20 cm height) placed within a sound proof chamber (Panlab, Barcelona, Spain). Different contexts were used: (A) white walls, metal grid on black floor, washed with 1% acetic acid, or (B) black walls, white rubber floor, washed with 70% ethanol). Mice were conditioned in context A. After 2 min habituation, mice received three pairings (60–120 s variable pairing interval) of a conditioned stimulus (CS: 4 kHz, 80 dB, 30 s tone) with an unconditioned stimulus (US: 2 s, 0.6 mA scrambled footshock) using a freezing system (Panlab). After 24 hours, contextual fear was tested by placing the mice in context A for 5 min and after another 24 hours, cued fear was tested by first placing the mice in context B for 2 min and after which the CS was presented twice (120 s intertrial interval). Freezing was measured using a load cell coupler (Panlab) and was defined as the lack of activity above a body weight-corrected threshold for a duration of 1 s or more as analyzed using Freezing software (Panlab).

Drug infusions. Drug infusions were made using an injection cannula (33 gauge, 3.5 mm, Plastics One). Immediately following fear conditioning, mice were gently scruffed and an injection cannula was inserted into each guide cannula. The injection cannulae were designed to protrude 1.0 mm from the tip of the guide cannula and effectively penetrated into the hippocampal CA3. Drugs or vehicle were infused at a flow rate of 0.10 µl per min and in a total volume of 0.25 µl per infusion site. Following infusion, the injection cannula was left in place for 1 min to allow drugs to diffuse from the cannula tip. Dummy cannulae were then inserted into each of the guide cannula and mice were returned to the homecage. At the end of each experiment, correct implantation of the guide cannulae was histologically verified on 40 µm slices obtained from brains fixed in 4% paraformaldehyde.

References

1 Chames, P., Van Regenmortel, M., Weiss, E., & Baty, D. *Br J Pharmacol* 157 (2), 220-233 (2009).
2 Sevigny, J. *et al. Nature* 537 (7618), 50-56 (2016).
3 Irannejad, R. *et al. Nature* 495 (7442), 534-538 (2013).
4 Hutchings, C.J., Koglin, M., & Marshall, F.H. *MAbs* 2 (6), 594-606 (2010).
5 Webb, D.R., Handel, T.M., Kretz-Rommel, A., & Stevens, R.C. *Biochem Pharmacol* 85 (2), 147-152 (2013).
6 Mujic-Delic, A., de Wit, R.H., Verkaar, F., & Smit, M.J. *Trends Pharmacol Sci* 35 (5), 247-255 (2014).
7 Jo, M. & Jung, S.T. *Exp Mol Med* 48, e207 (2016).
8 Steyaert, J. & Kobilka, B.K. *Curr Opin Struct Biol* 21 (4), 567-572 (2011).
9 Staus, D.P. *et al. Nature* 535 (7612), 448-452 (2016).
10 Jahnichen, S. *et al. Proc Natl Acad Sci U S A* 107 (47), 20565-20570 (2010).
11 Rasmussen, S.G. *et al. Nature* 477 (7366), 549-555 (2011).
12 Nicoletti, F. *et al. Neuropharmacology* 60 (7-8), 1017-1041 (2011).
13 Niswender, C.M. & Conn, P.J. *Annu Rev Pharmacol Toxicol* 50, 295-322 (2010).
14 Pin, J.-P. & Bettler, B. *Nature* 540 (7631), 60-68 (2016).
15 Moghaddam, B. & Adams, B.W. *Science* 281 (5381), 1349-1352 (1998).
16 Ferraguti, F. & Shigemoto, R. *Cell Tissue Res* 326 (2), 483-504 (2006).

17 Rondard, P., Goudet, C., Kniazeff, J., Pin, J.-P., & Prezeau, L. *Neuropharmacology* 60, 82-92 (2011).
18 Johnson, M.P. *et al. Psychopharmacology (Berl)* 179 (1), 271-283 (2005).
19 Nielsen, C.K. *et al. Med. Chem. Commun.* 2, 1120-1124 (2011).
20 Flor, P.J. & Acher, F.C. *Biochem Pharmacol* 84 (4), 414-424 (2012).
21 Gregory, K.J. & Conn, P.J. *Mol Pharmacol* 88 (1), 188-202 (2015).
22 Doumazane, E. *et al. FASEB J* 25 (1), 66-77 (2011).
23 Yin, S. *et al. J Neurosci* 34 (1), 79-94 (2014).
24 Pandya, N.J. *et al. Proteomics* (2016).
25 Hamers-Casterman, C. *et al. Nature* 363 (6428), 446-448 (1993).
26 Lauwereys, M. *et al. EMBO J* 17 (13), 3512-3520 (1998).
27 Behar, G. *et al. FEBS J* 276 (14), 3881-3893 (2009).
28 Doumazane, E. *et al. Proc Natl Acad Sci (USA)* 110 (15), 5754-5755 (2013).
29 Christopoulos, A. *et al. Pharmacol Rev* 66 (4), 918-947 (2014).
30 Scholler, P. *et al. Nat Chem Biol*, in press (2017).
31 Shigemoto, R. *et al. J Neurosci* 17 (19), 7503-7522 (1997).
32 Wright, R.A. *et al. Neuropharmacology* 66, 89-98 (2013).
33 Regehr, W.G. & Atluri, P.P. *Biophys J* 68 (5), 2156-2170 (1995).
34 Daumas, S., Ceccom, J., Halley, H., Frances, B., & Lassalle, J.M. *Learn Mem* 16 (8), 504-507 (2009).
35 Patil, S.T. *et al. Nat Med* 13 (9), 1102-1107 (2007).
36 Schaffhauser, H. *et al. Mol Pharmacol* 64 (4), 798-810 (2003).
37 Li, T. *et al. FASEB J* 26 (10), 3969-3979 (2012).
38 Moore-Morris, T. *et al. Mol Pharmacol* 75 (5), 1108-1116 (2009).
39 Fallarino, F. *et al. Nat Med* 16 (8), 897-902 (2010).
40 Nicoletti, F. *et al. Trends Pharmacol Sci* 28 (5), 206-213 (2007).
41 Alvarez-Rueda, N. *et al. Mol Immunol* 44 (7), 1680-1690 (2007).
42 El Moustaine, D. *et al. Proc Natl Acad Sci U S A* 109 (40), 16342-16347 (2012).
43 Trinquet, E. *et al. Anal Biochem* 358 (1), 126-135 (2006).
44 Sali, A. & Blundell, T.L. *J Mol Biol* 234 (3), 779-815 (1993).
45 Muto, T., Tsuchiya, D., Morikawa, K., & Jingami, H. *Proc Natl Acad Sci U S A* 104 (10), 3759-3764 (2007).
46 Larkin, M.A. *et al. Bioinformatics* 23 (21), 2947-2948 (2007).
47 Shen, M.Y. & Sali, A. *Protein Sci* 15 (11), 2507-2524 (2006).
48 Tsuchiya, D., Kunishima, N., Kamiya, N., Jingami, H., & Morikawa, K. *Proc Natl Acad Sci U S A* 99 (5), 2660-2665 (2002).
49 Monn, J.A. *et al. Journal of Medicinal Chemistry* 58 (4), 1776-1794 (2015).
50 Casciari, D., Seeber, M., & Fanelli, F. *BMC Bioinformatics* 7, 340 (2006).
51 Pierce, B.G., Hourai, Y., & Weng, Z. *PLoS One* 6 (9), e24657 (2011).
52 Feig, M., Karanicolas, J., & Brooks, C.L., 3rd. *J Mol Graph Model* 22 (5), 377-395 (2004).
53 Pettersen, E.F. *et al. J Comput Chem* 25 (13), 1605-1612 (2004).
54 Waterhouse, A.M., Procter, J.B., Martin, D.M., Clamp, M., & Barton, G.J. *Bioinformatics* 25 (9), 1189-1191 (2009).
55 Bischofberger, J., Engel, D., Li, L., Geiger, J.R., & Jonas, P. *Nat Protoc* 1 (4), 2075-2081 (2006).
56 Regehr, W.G. & Tank, D.W. *J Neurosci Methods* 37 (2), 111-119 (1991).

Figure 1

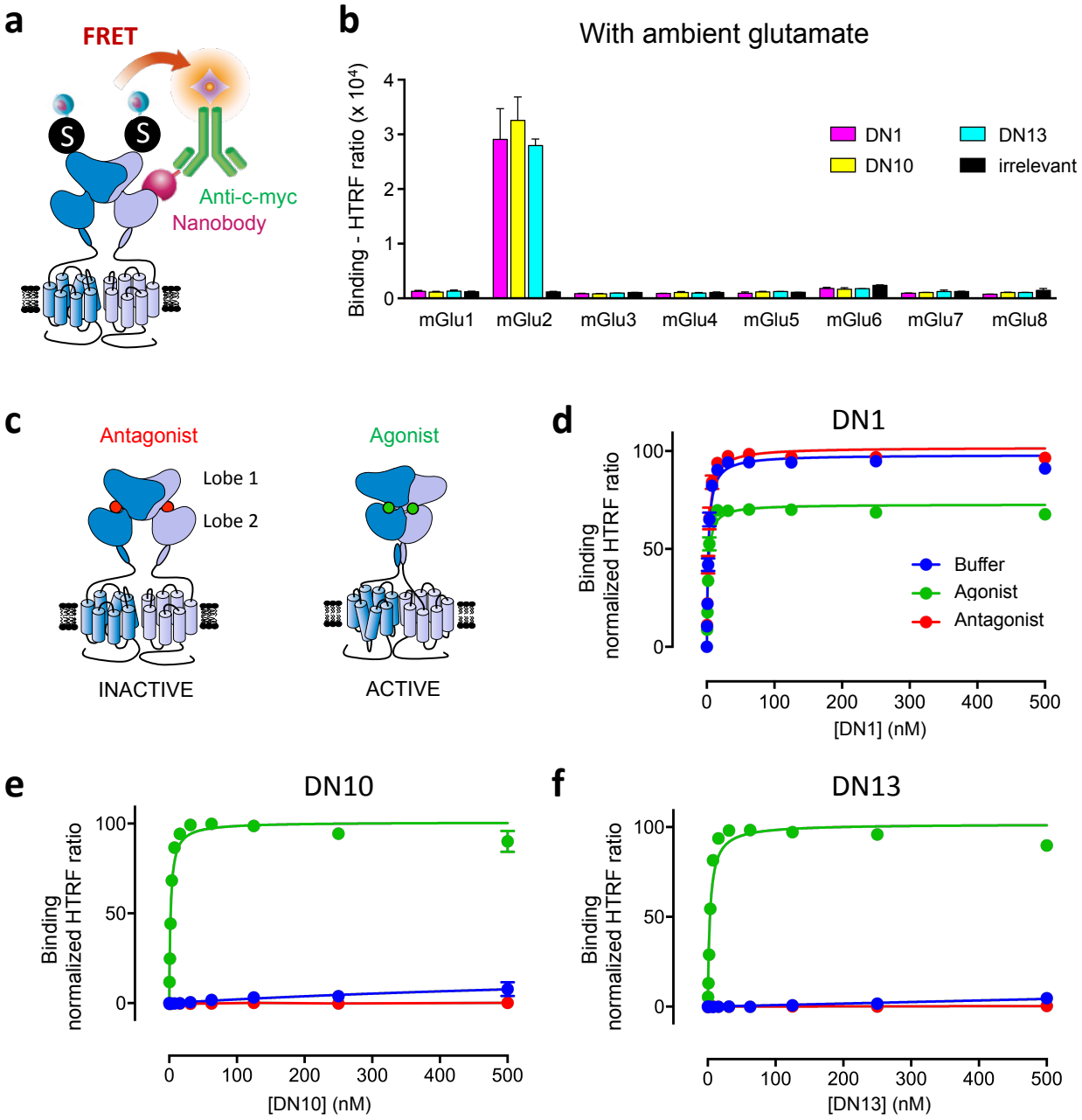

Figure 1: Nanobodies DN1, DN10 and DN13 specifically interact with mGlu2 receptors. **a)** Cartoon illustrating the principle of the TR-FRET binding assay. The receptor fused to a SNAP-tag (black circled labeled "S") is labeled with Lumi4-Tb (light blue ball) while the nanobody (purple) bearing a c-Myc epitope at its C-terminus is labeled with 200 nM of anti-c-Myc antibody (green) coupled to d2 fluorophores (orange). Binding of the nanobody to the receptor is then measured by a TR-FRET signal. **b)** Specific TR-FRET binding data obtained with the indicated mGlu receptor and either DN1, DN10, DN13 or a control irrelevant nanobody in cells under basal condition with ambient glutamate. Data are mean ± SD of triplicates from a typical experiment representative of three experiments. **c)** Cartoon illustrating the main active (left), and inactive (right) conformation of an mGlu2 dimer, stabilized by an agonist (glutamate or LY379268) or the antagonist LY341495, respectively. **d,e,f)** Saturation binding curves obtained with DN1 (**d**), DN10 (**e**) and DN13 (**f**) on mGlu2 receptors under control conditions with low extracellular glutamate thanks to the co-expression of the high affinity glutamate transporter EAAC1 (buffer), in the presence of the agonist LY379268 (1 µM), or the antagonist LY341495 (10 µM). Data are mean ± sem of three individual experiments each performed in triplicates.

Figure 2

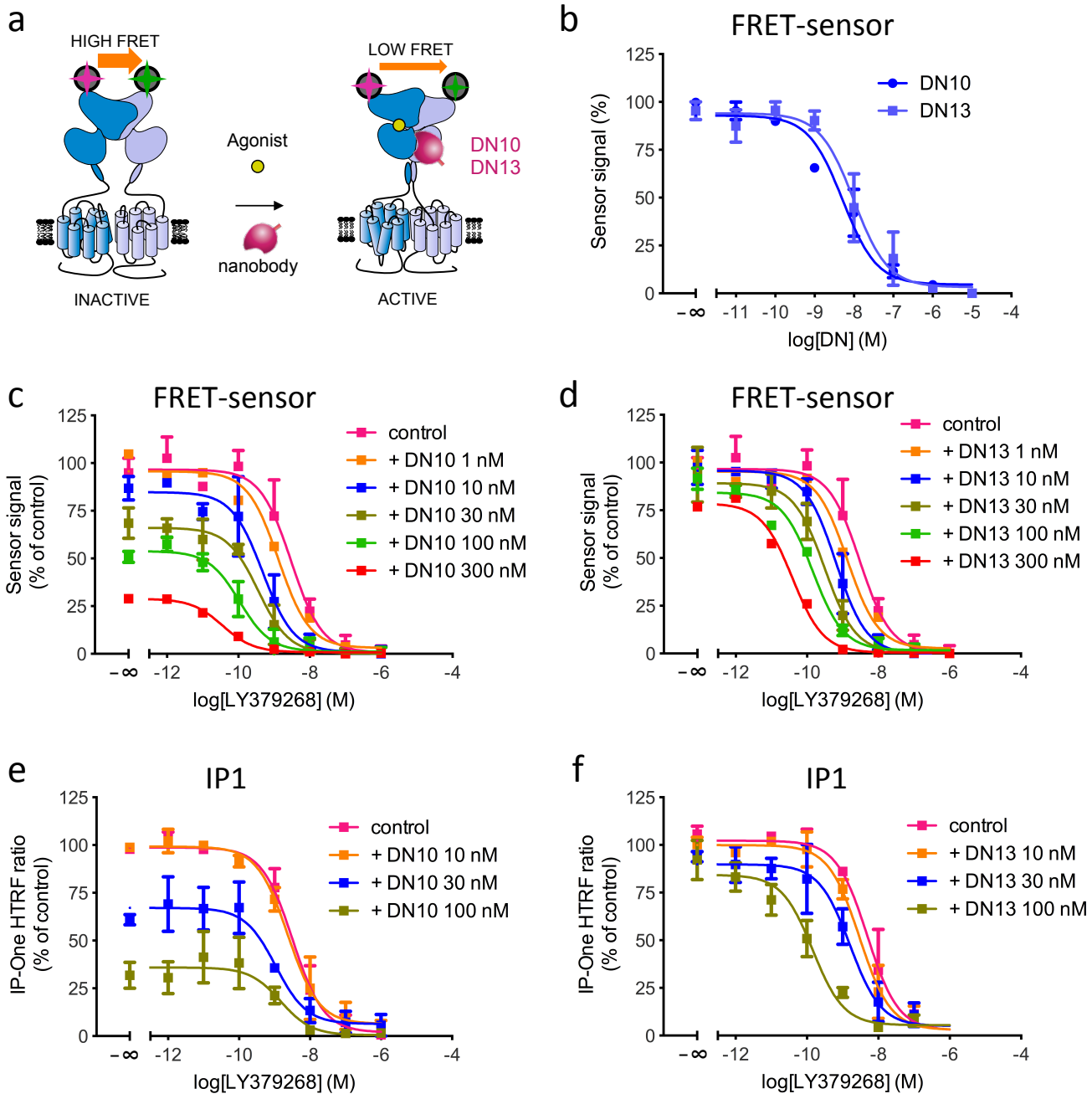

Figure 2: DN10 and DN13 are positive allosteric modulators of mGlu2. **a)** Cartoon illustrating the principle of the mGlu2 sensor assay, where the VFT movement associated with receptor activation results in a decrease in TR-FRET signal measured between Lumi4-Tb and SNAP-green labeled SNAP tags. **b)** DN10 and DN13 concentration dependent decrease the sensor signal in the presence of EC_{20} concentration of agonist LY379268 (0.1 nM), indicative of receptor activation. DN10 **(c)** and DN13 **(d)** dose-dependently potentiate the effect of LY379268 on the mGlu2 sensor. DN10 **(e)** and DN13 **(f)** dose-dependently potentiate the effect of LY379268 on the production of inositol phosphate in mGlu2-transfected cells. Note that the lower the IP-One HTRF ratio, the higher the amount of inositol monophosphate produced (IP1). Data are means ± sem of three individual experiments each performed in triplicates.

Figure 3

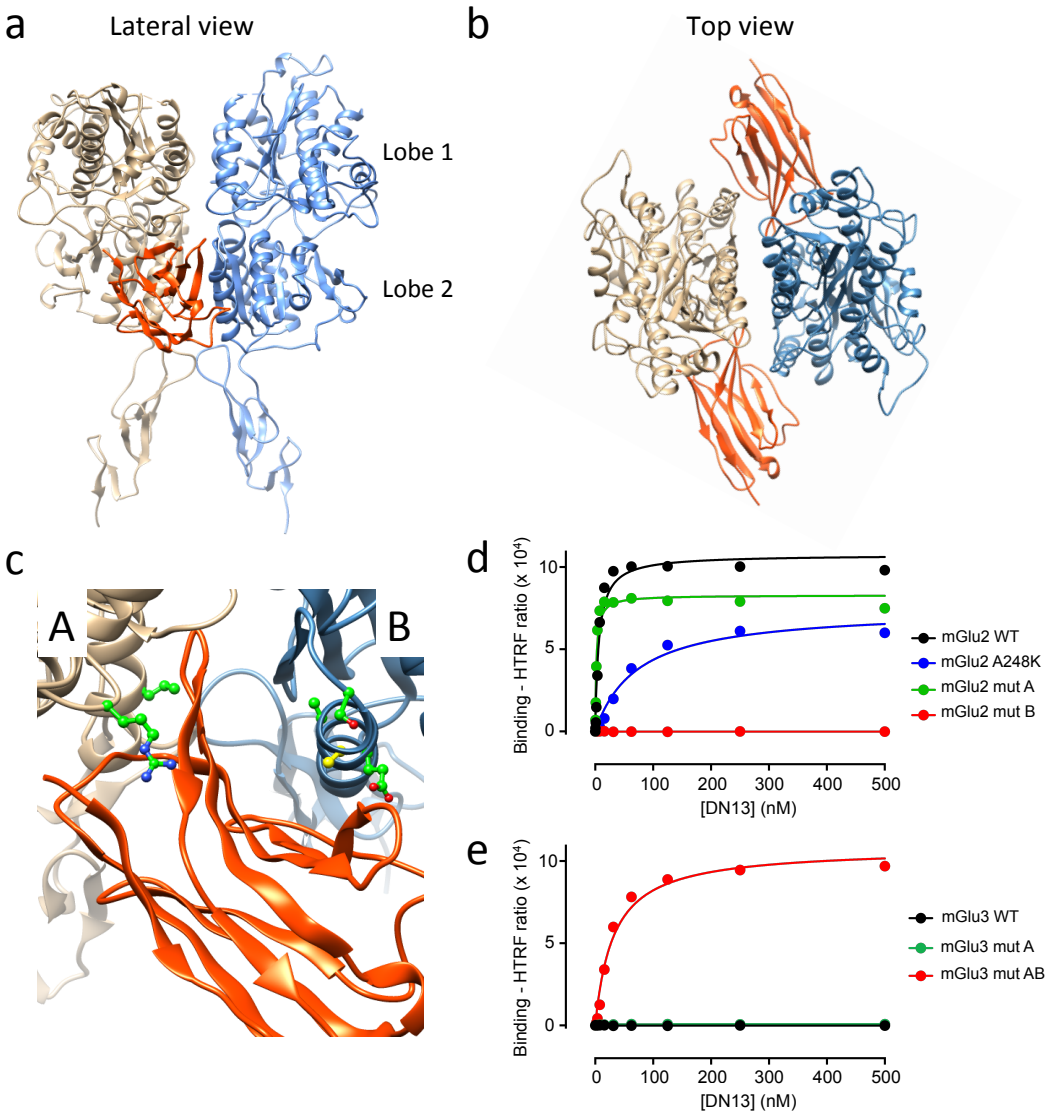

Figure 3: DN13 interacts at the lobe 2 crevice on the activated mGlu2 VFT dimer. **a-b)** View of the proposed docking of DN13 (orange) on the mGlu2 extracellular domain dimer (*a*, lateral view, *b*, top view). **c)** Detailed view of the proposed docking of DN13 illustrating proposed residues involved in selectivity, shown are Leu226 and Arg445 in protomer A, and Ser246, Ala248 (yellow), Ala249, and Glu251 from protomer B. **d)** Saturation binding curves of DN13 on mGlu2 WT, mGlu2 bearing mGlu3 specific residues from protomer A (mut A), mGlu2 bearing mGlu3 residues from protomer B (mut B), mGlu2 A248K mutant. **e)** Saturation binding curves of DN13 on mGlu3 WT, mGlu3 bearing the mGlu2 residues on protomer A (mut A), and mGlu3 bearing all identified residues of mGlu2 (mut AB). Data are mean ± SD of triplicates from a typical experiment representative of three experiments.

Figure 4

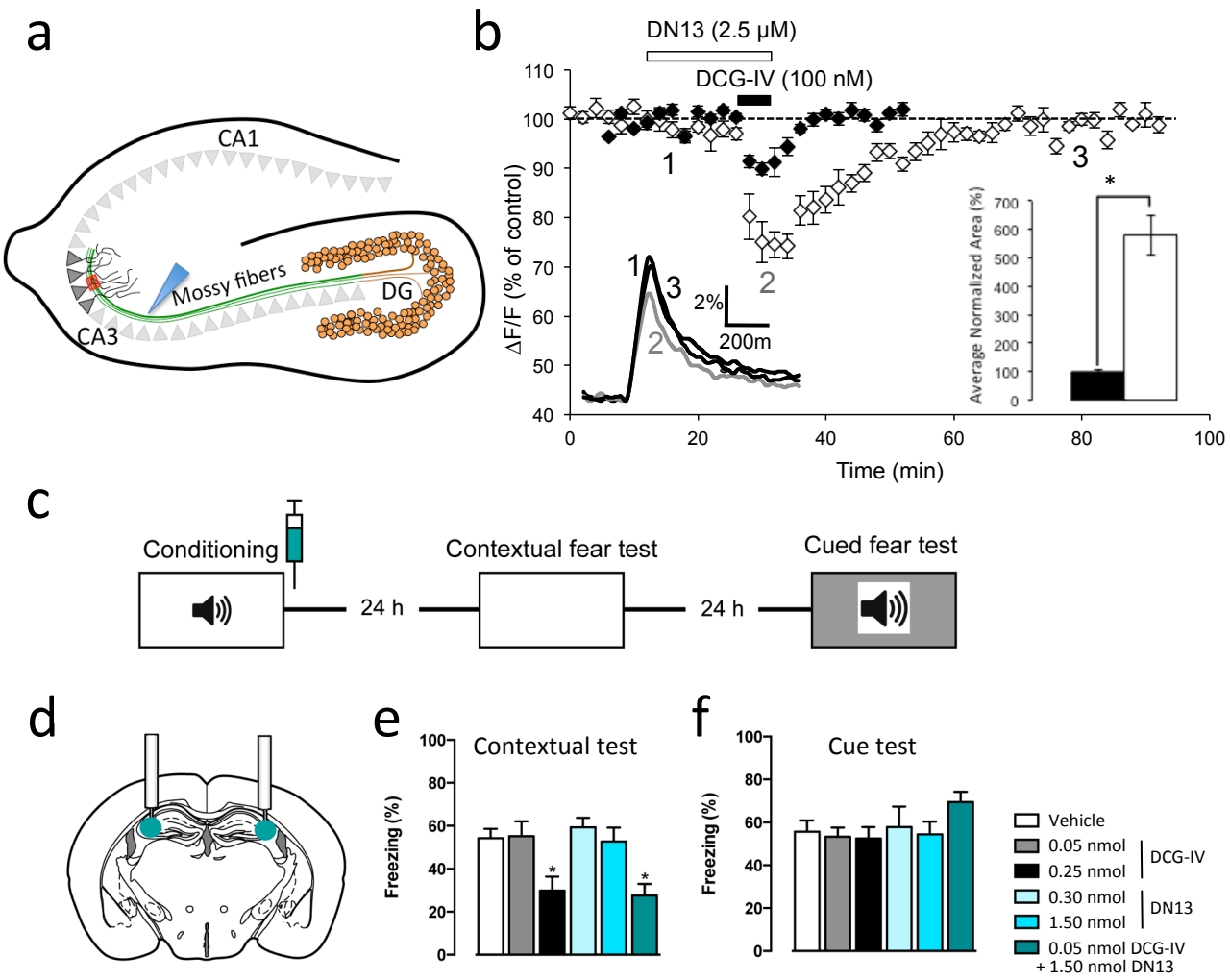

Figure 4: mGlu2 receptors in the CA3 area of the hippocampus control contextual fear consolidation. **a)** A schematic view of the hippocampus illustrating the granule neurons of the dentate gyrus (DG) projecting to the pyramidal neurons in the CA3 area via the mossy fibers. **b)** DN13 potentiates the inhibitory effect of a mGlu2-mGlu3 agonist (DCG-IV, 100 nM) on presynaptic evoked calcium transients in the CA3 area (red box in panel *a*) in response to electrical stimulation of the mossy fibers (blue arrow head in panel *a*). Data are normalized amplitudes of peak fluorescence transients (ΔF/F) evoked by five stimulations of mossy fibers (delivered at 100 Hz). Insert on the right shows the average normalized area corresponding to the depressant effect of DCG-IV alone (black bar, 100 ± 5.4%, n=10) and in the presence of DN13 (white bar, 578.5 ± 69%, n=9), p<0.001. Insert on the left displays superimposed fluorescence changes in one of these experiments recorded at the indicated times. Each trace is an average of 10 consecutive trials. Since the variance was different between DCG-IV and DCG-IV + DN13 groups, the Welch test was applied for statistical analysis. **c)** Schematic of the experimental protocol used for the contextual fear consolidation examination in mice, and drug infusion site **(d)**. **(e)** Contextual fear memory expression ANOVA: $F_{5,35} = 6.025$, P = 0.0004. **(f)** Cued fear memory. ANOVA: $F_{5,35} = 0.3053$, P = 0.9066. * P < 0.05 vs PBS and ** P < 0.01 vs PBS.